Structural and functional characterization of recombinant mouse annexin A11: influence of calcium binding

Emilio LECONA*, Javier TURNAY*, Nieves OLMO*, Ana GUZMÁN-ARÁNGUEZ*, Reginald O. MORGAN†, Maria-Pilar FERNANDEZ† and Mª Antonia LIZARBE*[1]

*Departamento de Bioquímica y Biología Molecular, Facultad de Ciencias Químicas, Universidad Complutense, 28040 Madrid, Spain, and †Departamento de Bioquímica y Biología Molecular, Facultad de Medicina, Universidad de Oviedo, 33006 Oviedo, Spain

Annexin A11 is one of the 12 vertebrate subfamilies in the annexin superfamily of calcium/phospholipid-binding proteins, distinguishable by long, non-homologous N-termini rich in proline, glycine and tyrosine residues. As there is negligible structural information concerning this annexin subfamily apart from primary sequence data, we have cloned, expressed and purified recombinant mouse annexin A11 to investigate its structural and functional properties. CD spectroscopy reveals two main secondary-structure contributions, α-helix and random coil (approx. 30 % each), corresponding mainly to the annexin C-terminal tetrad and the N-terminus respectively. On calcium binding, an increase in α-helix and a decrease in random coil are detected. Fluorescence spectroscopy reveals that its only tryptophan residue, located at the N-terminus, is completely exposed to the solvent; calcium binding promotes a change in tertiary structure, which does not affect this tryptophan residue but involves the movement of approximately four tyrosine residues to a more hydrophobic environment. These calcium-induced structural changes produce a significant thermal stabilization, with an increase of approx. 14 °C in the melting temperature. Annexin A11 binds to acidic phospholipids and to phosphatidylethanolamine in the presence of calcium; weaker calcium-independent binding to phosphatidylserine, phosphatidic acid and phosphatidylethanolamine was also observed. The calcium-dependent binding to phosphatidylserine is accompanied by an increase in α-helix and a decrease in random-coil contents, with translocation of the tryptophan residue towards a more hydrophobic environment. This protein induces vesicle aggregation but requires non-physiological calcium concentrations *in vitro*. A three-dimensional model, consistent with these data, was generated to conceptualize annexin A11 structure–function relationships.

Key words: calcium binding, CD spectroscopy, fluorescence spectroscopy, phospholipid binding, thermal stability.

INTRODUCTION

The annexin gene family comprises calcium-binding proteins with a unique ancestry, a tetrad structure of homologous internal repeats, and the common property of reversible binding to acidic phospholipid-rich membranes in the presence of this cation (see [1–3] for reviews), although some protein members lack the requisite consensus for high-affinity type II calcium-binding sites [4]. The annexin core structure is composed of four (eight in annexin A6) homologous domains of approx. 68 amino acids, universally conserved throughout annexin evolution [5,6]. In contrast, the N-terminal region shows greater variability in length and amino acid sequence [1,3]. Since the solution of the annexin A5 crystal structure [7], several other annexins have been crystallized; all of them display a protein core resembling a slightly curved disc in which the four repeated domains arrange around a central hydrophilic pore. Each domain comprises a folded leaf α-helix bundle (helices A, B, D and E) organized as anti-parallel cylinders capped by a fifth α-helix (helix C). The interaction with membranes takes place on the convex side of the molecule where the principal calcium-binding sites are located. Calcium binding is established with carbonyl oxygen atoms in the loop connecting helices A and B, and with a bidentate carbonyl group from glutamic or aspartic residues located in the loop connecting helices D and E, approx. 38 residues downstream in each repeat. The N-terminal region connects domains I and IV in annexins with a short N-terminus, such as annexin A5, and is located in the concave region of the molecule, opposite to the calcium-binding sites [7]. Rosengarth et al. [8] have solved the X-ray structure of full-length annexin A1 in the absence of calcium, showing that the N-terminus interacts with domain III through an amphipathic α-helix present in the N-terminal domain replacing helix 3D.

The structural characteristics of annexins, especially A1, A2 and A5, have been extensively analysed [7–12]. However, knowledge is more limited for other members of this family, and is unavailable for annexin A11 which has an unusual N-terminus. The core domain of annexin A11 shows the highest similarity to all other human annexins [13,14] and its evolutionary origin lies near the root of this family tree [6,15], beginning with the sequential duplication of annexin A13 to annexins A7 and A11 around the emergence of chordates [16,17]. All these observations support the view of annexin A11 as a structural prototype, founding member and key functional model of chordate annexins.

Several functions have been described for annexins *in vitro*, including anti-coagulatory and anti-inflamatory activities and involvement in signal transduction, membrane fusion, endo- and exocytosis as well as calcium-channel regulation. However, little is known about their physiological role *in vivo* [1,3]. Despite their gross structural similarity, annexins have diverged

Abbreviations used: CCA, convex constraint algorithm; DTT, dithiothreitol; IPTG, isopropyl β-D-thiogalactoside; Ni-NTA, Ni^{2+}-nitrilotriacetate; PA, phosphatidic acid; PC, phosphatidylcholine; PE, phosphatidylethanolamine; PG, phosphatidylglycerol; PS, phosphatidylserine; rTEV, recombinant tobacco etch virus.

[1] To whom correspondence should be addressed (e-mail lizarbe@bbm1.ucm.es).

significantly in terms of their gene regulation, tissue-specific expression patterns, subcellular localization of different isoforms and features peculiar to individual subfamilies [16,18–20]. Moreover, self-association, heterologous annexin interactions and the interaction with other proteins have been described to act as regulatory mechanisms for the function of some of these proteins [1–3].

The main structural differences among metazoan annexins appear in the non-homologous N-terminal extension, so the structural analysis of annexin A11 could reveal some features relevant to its functional specificity. This annexin possesses an extensive N-terminal region, rich in proline, glycine and tyrosine residues [21,22]. Although several studies have pointed out various functional properties of annexin A11, including its possible role in insulin secretion [23], structural data are limited to the primary structure. The N-terminal region of annexin A11 has been proposed to be responsible for its autoantigenicity [24], nuclear localization [25] and tyrosine phosphorylation [26]. Moreover, the interaction with calcyclin (S100A6) is established through amino acids 45–62 [27], analogous to that described for annexins A1 and A2 with other S100 proteins, namely S100A11 and S100A10, or for p53 with S100B [28–30]. Annexin A11 also binds, through the N-terminus, to the penta-EF-hand family proteins *ALG-2* (apoptosis-linked gene-2) [31] and sorcin [32].

According to all these observations, annexin A11 is probably involved in several biological processes and its N-terminal region participates prominently in most of them. The aim of the present study is to perform a structural characterization of recombinant annexin A11 to allow a better understanding of the biological role of this protein. We have analysed some of the changes that take place on calcium binding as this is a key aspect of its functionality. We also studied the binding of annexin A11 to different phospholipid vesicles, as well as the consequent structural changes, to gain insight into the interaction of this protein with biological membranes, as this process may differ from other annexins due to its distinctive N-terminus.

EXPERIMENTAL

Construction of expression vectors

The mouse annexin cDNA was cloned previously (U65986) [14]. The 2.4 kb clone containing the full-length cDNA sequence was used as a template to isolate the coding portion of mouse annexin A11 by PCR. Oligonucleotide primers, 23 bp long, were synthesized according to the published sequence for both ends of the coding cDNA. The oligonucleotide sequences created *Nco*I and *Eco*RI restriction sites to facilitate the insertion of coding cDNA into either expression plasmid pPROEX-HTb (Life Technologies, Prat de Llobregat, Spain) or pTrc99A (AP Biotech, Cerdanyola, Spain). The identities of the final constructs pHisA11M and pTrcA11M were verified by restriction digestion and DNA sequencing.

Protein expression and purification

JA221 *Escherichia coli* cells were transformed with the annexin A11 expression constructs pTrcA11M or pHisA11M. Cells were grown at 37 °C in Luria–Bertani medium containing 100 μg/ml ampicillin until the cultures reached A_{600} 0.5. Recombinant protein expression was induced by the addition of 1 mM isopropyl β-D-thiogalactoside (IPTG) for different incubation times (1–16 h) and at temperatures over the range 25–37 °C. The protein expression of total cell homogenates was analysed by SDS/PAGE and then by Coomassie Blue staining or Western blotting. Optimal conditions for the induction of the expression of recombinant annexin A11 in both cases were 4 h in the presence of 1 mM IPTG at 25 °C.

Spectroscopic characterization was performed using recombinant annexin A11 produced in bacteria transformed with the construction pHisA11M under the optimal expression conditions described above. Cells were collected after induction with IPTG by centrifugation at 6000 ***g*** for 15 min and resuspended in 50 mM Tris (pH 8.0), containing 0.1 M NaCl, 2.5 mM EGTA, 2 mM PMSF and 1 mM dithiothreitol (DTT), and ruptured by sonication cycles at 4 °C. After stirring for 90 min at 4 °C, the homogenate was centrifuged at 27000 ***g*** for 90 min at 4 °C. The supernatant was loaded on to an Ni^{2+}-nitrilotriacetate (Ni-NTA)–agarose column, washed with buffer A [50 mM Tris (pH 8.0)/0.1 M NaCl/1.5 mM 2-mercaptoethanol] containing 20 mM imidazole. The recombinant protein was eluted with a linear gradient of buffer A containing 20–250 mM imidazole, and dialysed against 50 mM Tris (pH 8.0), containing 0.1 M NaCl and 1 mM EGTA. After the addition of 1 mM DTT, the protein was digested with 10 units/ml recombinant tobacco etch virus (rTEV) protease (Life Technologies) at 4 °C for 20–22 h and dialysed against buffer B [50 mM Tris (pH 8.0)/0.1 M NaCl]. Digested annexin was separated from the undigested form and from the rTEV protease by an additional Ni-NTA–agarose affinity chromatography, taking advantage of the presence of a poly(His) tag in the latter molecules. Finally, annexin A11 was dialysed against buffer B containing 1 mM EGTA, to remove traces of Ni^{2+} that induce alterations in the UV–visible spectra, and then against buffer B without EGTA.

The identity of both digested and non-digested proteins was confirmed by amino acid analysis (Beckman 6300 amino acid analyser) as described previously [33], which also allowed the determination of protein concentration. The molar absorption coefficient at 280 nm was obtained from the UV–visible spectra, after subtraction of apparent absorption due to light scattering and determination of the protein concentration by amino acid analyses from aliquots taken directly from the cuvette.

CD measurements

CD spectra were recorded at 20 °C in a Jasco J-715 spectropolarimeter equipped with a Neslab RTE-111 thermostat. The far-UV CD spectra were monitored between 200 and 250 nm using thermostatically controlled cuvettes of 0.1 cm pathlength. Melting curves were determined by monitoring the ellipticity changes at 208 or 220 nm between 20 and 80 °C at 60 °C/h. All the samples were first dialysed against 20 mM Hepes (pH 8.0) and 0.1 M NaCl, to minimize pH changes during heating. To analyse the influence of calcium concentration on the far-UV spectrum and on the melting temperature (T_m), different protein samples from the same stock were prepared with increasing $CaCl_2$ concentrations up to 75 mM. Samples with equivalent maximal ionic strength, obtained by the addition of NaCl instead of $CaCl_2$, were used as the control. Far-UV spectra and melting temperatures were also registered for annexin A11 in the presence of 50 nm phosphatidylserine (PS) small unilamellar vesicles (molar ratio of PS/annexin A11 is 800 : 1), in the absence (1 mM EGTA) or presence of 200 μM $CaCl_2$.

All spectra were averaged over six scans (ten for annexin A11 in the presence of vesicles) and were corrected by subtracting buffer contribution (with or without PS vesicles) from parallel spectra in the absence of protein; units are always expressed as molar ellipticity/residue ($[\theta]_{MRW}$). Prediction of the secondary structure from the far-UV spectra was performed using the convex constraint algorithm (CCA) as described by Perczel et al. [34].

Fluorescence spectroscopy

Fluorescence emission spectra were recorded at 20 °C on an SLM Aminco 8000C spectrofluorimeter with excitation wavelengths of 275 nm (global emission) and 295 nm (tryptophan emission), and 4 nm excitation and emission bandwidths. The spectra were monitored between 295 and 400 nm for global emission or 305 and 400 nm for tryptophan emission, using a 0.4 cm excitation pathlength and 1.0 cm emission pathlength cuvette. Scattering was minimized by crossed Glan–Thompson polarizers. Titration of calcium influence at both excitation wavelengths was performed by sequential addition of $CaCl_2$ in the absence or presence of 50 nm PS vesicles (molar ratio of PS/annexin A11 is 800 : 1) and correcting the spectra for dilution. Acrylamide quenching of tryptophan fluorescence was measured using emission spectra exciting at 295 nm at increasing acrylamide concentration, taking into account the effects of dilution as described previously [9]. Care was taken to avoid the inner filter effect and the solutions presented always UV absorption at the excitation wavelength below 0.04. The Stern–Volmer quenching constant (K_{SV}) was calculated from the plot of F_0/F at 340 nm against acrylamide concentration, according to the equation $F_0/F = 1 + K_{SV}[Q]$, where F_0 is the fluorescence intensity at zero quencher concentration and F the intensity at a given quencher concentration ([Q]).

Tyrosine titration

Titration was performed by the addition of aliquots of 1 M NaOH to the protein sample in the absence or presence of 50 mM $CaCl_2$, using a 1 cm pathlength cuvette. After each addition, the pH was measured in the cuvette with a microelectrode and the UV–visible absorption spectrum was recorded. Absorption at 295 nm due to tyrosinate was determined after subtraction of the apparent absorption due to light scattering and taking into account the dilution of the sample. The number of tyrosine residues titrated at each pH was calculated from the molar ratio [tyrosinate]/[annexin A11], and the plot of this value against pH renders the titration curve.

Binding to phospholipids and vesicle aggregation assays

Unilamellar vesicles of PS (Avanti Polar Lipids), phosphatidylcholine (PC), phosphatidylglycerol (PG), phosphatidic acid (PA) and phosphatidylethanolamine (PE) (all purchased from Sigma) were obtained by hydration of a thin film of dried phospholipids in 50 mM Tris (pH 8.0) containing 0.1 M NaCl, followed by sonication and extrusion through polycarbonate filters of either 100 or 400 nm (Lipex Biomembranes). PE vesicles were stabilized by the addition of PC (PE/PC in the ratio 4 : 1) to avoid artifacts due to the formation of hexagonal-phase structures in pure PE liposomes. Small unilamellar vesicles (50 nm) were prepared from freshly obtained 400 nm vesicles by further extrusion through 50 nm polycarbonate filters.

Purified annexin A11 and 400 nm vesicles were mixed in a lipid/protein constant molar ratio of 800 : 1 with variable calcium concentrations in 50 mM Tris (pH 8.0) and 0.1 M NaCl and kept at room temperature (20 °C) for 15 min. The final mixture (300 μl) was ultracentrifuged at 134000 ***g*** at 4 °C for 1 h (Airfuge Beckman); the pellet and the supernatant were separated and analysed by SDS/PAGE followed by silver nitrate staining or Western blotting. Under these experimental conditions, almost no sedimentation of free protein was detected in a phospholipid-free control. Gels or films were scanned and densitometric analysis was performed, obtaining volumograms on a photodocumentation system obtained from UVItec (Cambridge, U.K.) and using the UVIBand V.97 software.

Vesicle aggregation was studied using 100 nm vesicles (obtained by extrusion through 100 nm polycarbonate filters; 0.1 mg/ml PS) in the presence of increasing annexin A11 concentrations at 25 °C and triggering the reaction by adding the corresponding volume from a concentrated $CaCl_2$ stock solution. Absorption at 360 nm was measured immediately after the addition of calcium in a thermostatically controlled cuvette for at least 10 min.

Other procedures

The isolation of chicken annexin A5 was performed as described previously [9,35]. SDS/PAGE was performed by the method of Laemmli [36]. Western blotting was performed as described previously [37] using either polyclonal anti-bovine annexin A11 antibodies (dilution 1:8000; kindly provided by Dr Hiroyoshi Hidaka, D. Western Therapeutics Institute, Nagoya, Japan) and a secondary antibody conjugated with horseradish peroxidase (Bio-Rad, Madrid, Spain), or using directly a monoclonal peroxidase-conjugated anti-poly(His) (Sigma). Polyclonal antibodies against recombinant mouse annexin A11 were raised in rabbit following standard methods. Annexin A11 concentration in pure preparations was determined from the UV–visible spectra, except for CD spectroscopy, where quantitative amino acid analysis was used. Regression fitting of the experimental data to different equations was performed using SigmaPlot software v.8.02 obtained from SPSS (Chicago, IL, U.S.A.).

RESULTS

Purification of recombinant mouse annexin A11

The expression of recombinant annexin A11 cloned in the vector pTrc99A is low in all the experimental conditions assayed; the protein is extensively degraded even at 25 °C and short induction times, and is mainly expressed in an insoluble form. On the other hand, the cloning of the protein in the vector pPROEX-HTb, which introduces a His tag in the N-terminus, allows a significantly greater expression and minimizes degradation. According to the Western blots, using antibodies against the wild-type protein or against the poly(His) tag (Figure 1A), the degradation of the protein takes place from the N-terminus. Moreover, the His tag enables easy purification of annexin A11 expressed in *E. coli* at 25 °C for 4 h.

Figures 1(B) and 1(C) show the electrophoretic and Western-blot analyses of samples from the main steps of the purification process. Bacteria were collected by centrifugation and homogenized in the presence of 2.5 mM EGTA to obviate interactions of the recombinant annexin with bacterial membrane phospholipids and 1 mM DTT to prevent incorrect disulphide bond formation. Centrifugation of the cell homogenate allows the separation of the soluble and insoluble fractions (Figures 1B and 1C, lanes j–l). Approx. 50 % of the recombinant annexin A11 remains insoluble either in inclusion bodies or associated with the membrane fraction. After removing EGTA by dialysis, the soluble fraction was purified by affinity chromatography in Ni-NTA–agarose. Whereas bacterial proteins do not bind to Ni-NTA–agarose (Figures 1B and 1C, lane m), annexin A11 with the His tag elutes only in the presence of imidazole (Figures 1B and 1C, lane n). Removal of imidazole by dialysis in the absence

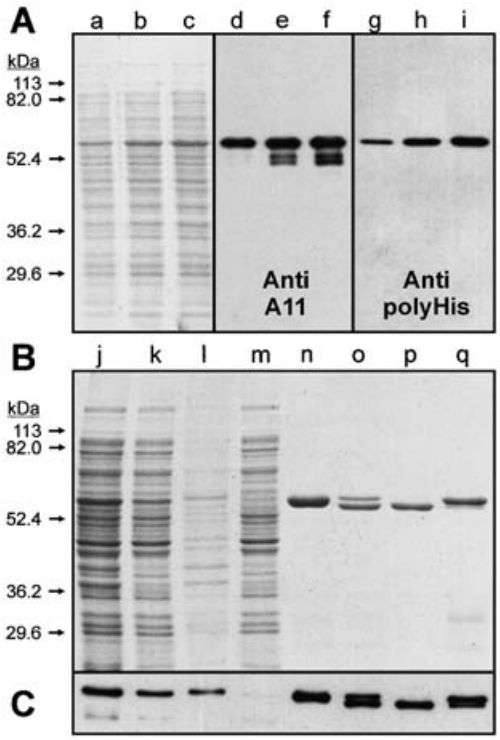

Figure 1 SDS/PAGE analysis of recombinant annexin A11 expression and purification

(**A**) Expression of annexin A11 was induced in exponentially growing JA221 cells by the addition of 1 mM IPTG and incubation at 25 °C for 4 h (lanes a, d and g), 6 h (lanes b, e and h) and 8 h (lanes c, f and i), and the expression was analysed by SDS/PAGE followed by Coomassie Blue staining (lanes a–c) and Western blotting using antibodies raised against either bovine annexin A11 (lanes d–f) or the poly(His) tag (lanes g–i). Purification of recombinant annexin A11 from bacterial cultures induced for 4 h with 1 mM IPTG at 25 °C was performed, followed by SDS/PAGE analysis and Coomassie Blue staining (**B**) and Western-blot analysis with anti-(annexin A11) antibodies (**C**). (**B**, **C**) Lane j, bacterial homogenate after protein expression induction; lanes k and l, supernatant and sediment respectively after centrifugation of the homogenized material in the presence of 2.5 mM EGTA; lane m, flow-through of the Ni-NTA chromatography; lane n, pool of fractions containing annexin A11; lane o, digestion of poly(His) tag containing annexin A11 with rTEV protease; lane p, purified digested annexin A11 without the poly(His) tag; lane q, material retained in the Ni-NTA–agarose chromatography after digestion with rTEV protease.

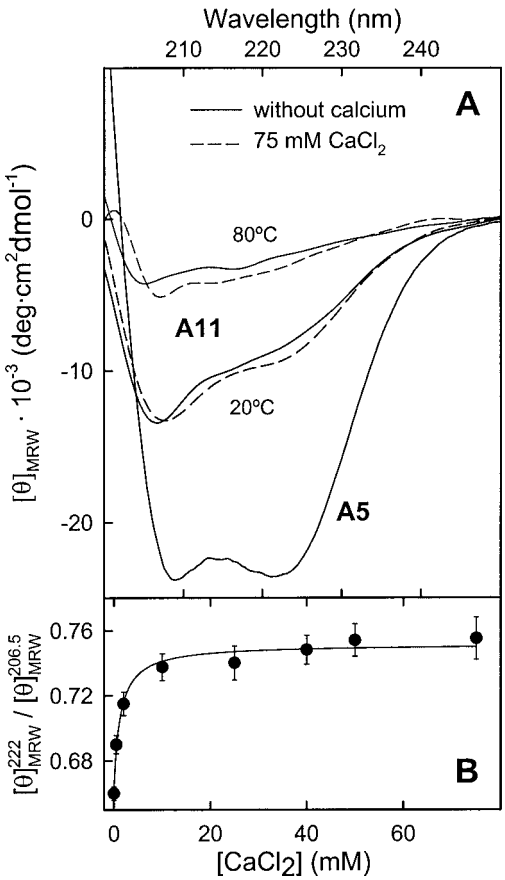

Figure 2 Far-UV CD spectra of annexin A11

(**A**) Representative far-UV CD spectra of annexin A11 without calcium (——) and in the presence of 75 mM $CaCl_2$ (– – –) at 20 and 80 °C are shown in comparison with that of chicken annexin A5 at 20 °C in the absence of calcium, and were registered in 50 mM Hepes (pH 8.0) and 0.1 M NaCl. (**B**) Variation in the ratio between molar ellipticities/residue at 222 and 206.5 nm with calcium concentration. Results are expressed as means ± S.D. for at least three different spectra (each of them averaged over six scans).

of bivalent-cation chelating agents induces the autoaggregation and precipitation of the protein containing the His tag; a similar process takes place if calcium is added to solutions of this protein. As this tag is likely to be involved in the autoaggregation of the protein, this extension was removed to perform the spectroscopic characterization of the protein. Digestion of the protein for 20 h at 4 °C in the presence of 10 units/ml rTEV protease yielded over 70 % of digested protein (Figures 1B and 1C, lane o). Separation of the digested annexin A11 from the undigested protein and from the enzyme was achieved by a further chromatographic step in Ni-NTA–agarose; the protease and the undigested annexin A11 are bound to the resin, whereas the digested protein elutes in the flow-through (Figures 1B and 1C, lanes p and q).

Identity of the purified proteins was confirmed through amino acid analyses and antibodies against the recombinant protein recognized wild-type annexin A11 from cell extracts in the Western blot. The molar absorption coefficient (51761 $M^{-1} \cdot cm^{-1}$) was determined from the absorption spectrum in the UV–visible region after correction for apparent absorption and determination of protein concentration by amino acid analysis.

CD analysis

The CD spectrum of annexin A11 in the far-UV region is shown in Figure 2(A) in comparison with the spectrum of chicken annexin A5 as reference. Annexin A11 in the absence of calcium presents a minimum at 206.5 nm with a molar ellipticity/residue of -13440 degrees $\cdot cm^2 \cdot dmol^{-1}$. This spectrum differs significantly from that of annexin A5, which has a relatively short N-terminal extension of approx. 15 residues and whose spectrum in the absence of calcium presents two minima at 208 and 222 nm showing much higher negative molar ellipticities. The contribution of the different secondary-structure elements, calculated according to the CCA method, reveals that whereas annexin A5 possesses over 70 % of α-helix, the main contributions to annexin A11 structure are α-helix (29 %), random coil (31 %) and β-turns (26 %).

Calcium concentrations required for reproducing the annexin conformational rearrangements induced in the absence of phospholipids are almost three orders of magnitude higher than those required in their presence [1,2,10]. Hence, calcium concentrations in the millimolar range were used throughout these experiments. Addition of calcium to annexin A11 induces small but significant changes in the far-UV CD spectrum. Figure 2(A) also shows the spectrum of annexin A11 saturated

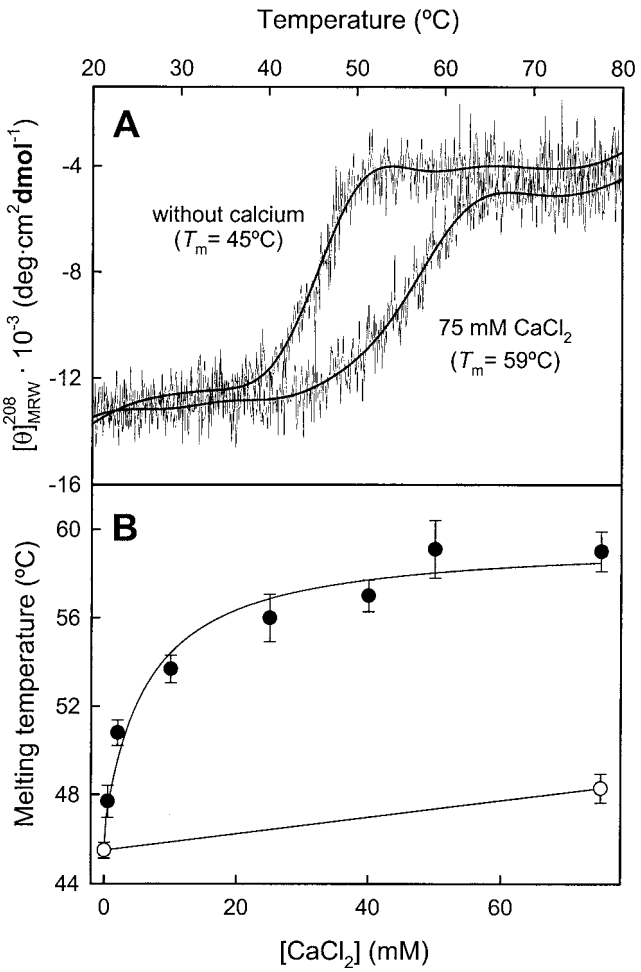

Figure 3 Influence of calcium binding on the thermal stability of annexin A11

(**A**) Melting curves of annexin A11 in the absence or in the presence of 75 mM $CaCl_2$ in 20 mM Hepes (pH 8.0) and 0.1 M NaCl. The original unsmoothed data are presented as thin lines together with the results from noise reduction using the Standard Analysis software obtained from Jasco. (**B**) Dependence of the melting temperature on $CaCl_2$ concentration (●) was analysed by determining T_m values at different calcium concentrations. Results represent the means ± S.D. for at least two independent determinations at each $CaCl_2$ concentration. ○, effect of an increase in ionic strength using an NaCl concentration equal to the highest $CaCl_2$ concentration.

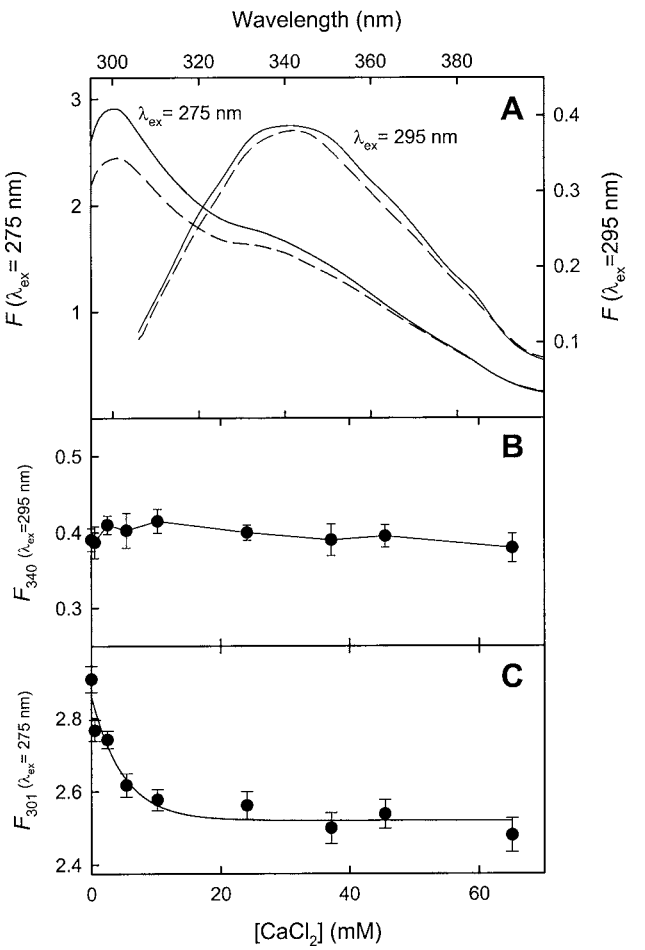

Figure 4 Fluorescence emission spectra of annexin A11 after calcium binding

(**A**) Emission spectra at excitation wavelengths of 275 and 295 nm in the absence of calcium (——) or presence of 75 mM $CaCl_2$ (– – –) were registered at 25 °C at 295–410 nm (λ_{ex} = 275 nm) or 305–410 nm (λ_{ex} = 295 nm). Fluorescence is expressed in arbitrary units; the scale for fluorescence emission at an excitation wavelength of 295 nm has been expanded (right axis). Variations in the fluorescence intensity in the emission maxima of tryptophan (340 nm, λ_{ex} = 295 nm) and tyrosine (301 nm, λ_{ex} = 275 nm) with calcium concentration have been plotted in (**B**) and (**C**) respectively.

with calcium (75 mM $CaCl_2$; molar ratio of calcium/protein is approx. 80000 : 1). These changes are not induced by the increase in the ionic strength of the solvent, since no changes in the spectrum are observed when NaCl concentration is increased up to 325 mM, equivalent to the presence of 75 mM $CaCl_2$ in a buffer containing 100 mM NaCl. Comparison of the spectra in the absence and presence of 75 mM $CaCl_2$ shows a shift in the minimum from 206.5 to 208 nm; this shift is already observed at 2 mM $CaCl_2$ and is maintained at higher calcium concentrations. Moreover, a gradual increase in the ratio between molar ellipticities at 222 and 206.5 nm is observed, showing a hyperbolic dependence with the calcium concentration (Figure 2B). These changes suggest a slight increase in α-helix content induced by calcium binding. In fact, CCA analysis of the spectrum at 75 mM calcium yields a 5 % increase in the secondary structure (approx. 34 %), with a parallel decrease in random coil (approx. 24 %).

Thermal stability

The stability of annexin A11 was analysed by monitoring the molar ellipticity at 208 nm as a function of temperature. In the absence of calcium, the melting curve shows a co-operative unfolding of the protein with a T_m of approx. 45 °C (Figure 3A). The binding of calcium by annexin A11 induces a highly significant increase in the thermal stability of the protein; in the presence of 75 mM $CaCl_2$, there is an increase of approx. 14 °C in the T_m, with a slight loss of co-operativity (Figure 3A). The variation in the T_m with calcium concentration can be adjusted to a rectangular hyperbola, showing a midpoint effect at 6.3 mM (Figure 3B). Thermal stabilization induced by calcium is specific and is not due to alterations in the polarity of the solvent, as an increase in ionic strength with NaCl up to 325 mM induces only a slight increase in the T_m of approx. 2.8 °C.

Fluorescence emission analysis

Figure 4(A) shows the fluorescence emission spectra of annexin A11 at excitation wavelengths of 275 and 295 nm in the absence

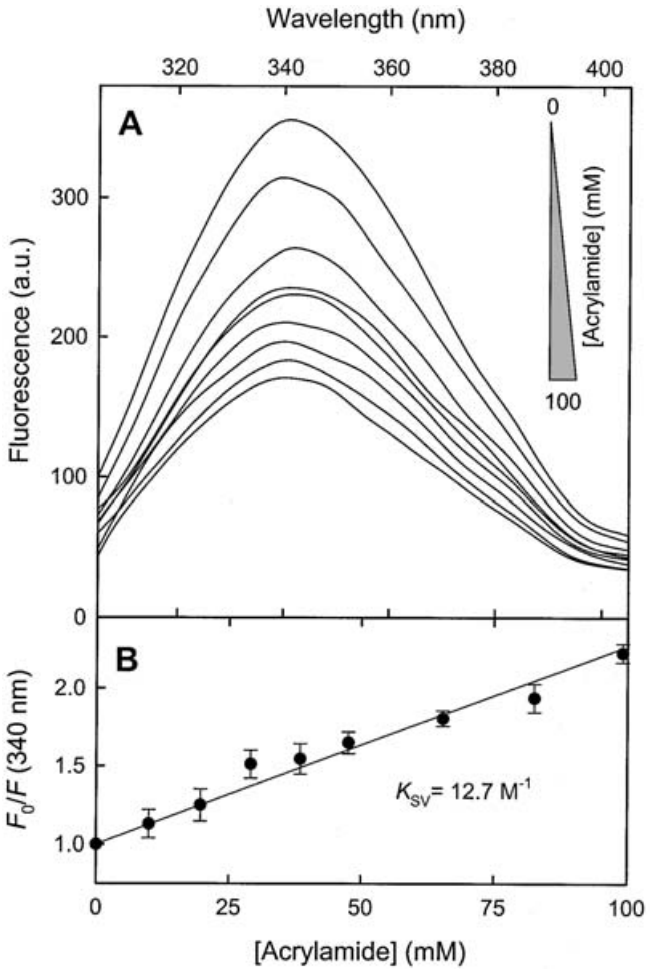

Figure 5 Acrylamide quenching of tryptophan emission

Fluorescence emission ($\lambda_{ex} = 295$ nm) at 20 °C of the unique tryptophan residue in annexin A11 was quenched by sequential addition of a concentrated acrylamide stock solution up to 100 mM. A representative experiment is shown in (**A**). Fluorescence intensities at 340 nm were plotted against acrylamide concentration and fitted to the Stern–Volmer equation (**B**). Results are expressed as means ± S.D. for three independent experiments.

of calcium or in the presence of 75 mM $CaCl_2$. The maximum in the fluorescence emission spectrum of the unique tryptophan residue of annexin A11 (Trp^{23}) appears at 340 nm and its position was not altered when calcium was added to the solvent, and no significant changes were observed in the quantum yield of this residue up to 75 mM $CaCl_2$ (Figure 4B). A maximum in the fluorescence emission spectrum at 301 nm is obtained using an excitation wavelength of 275 nm. This maximum is almost exclusively due to tyrosine residues and its position is not altered in the presence of calcium. However, as shown in Figure 4(C), a hyperbolic decrease of approx. 15 % in the quantum yield of these residues is observed in a calcium concentration-dependent manner, showing a midpoint at 3.4 mM $CaCl_2$, and this effect is almost saturated at concentrations higher than 20 mM.

Acrylamide quenching of tryptophan emission

To analyse the degree of exposure to the solvent of Trp^{23}, we have studied the effect of acrylamide on the fluorescence emission spectrum obtained at an excitation wavelength of 295 nm. Figure 5(A) shows the emission spectra of the tryptophan residue at increasing acrylamide concentrations up to 100 mM, which

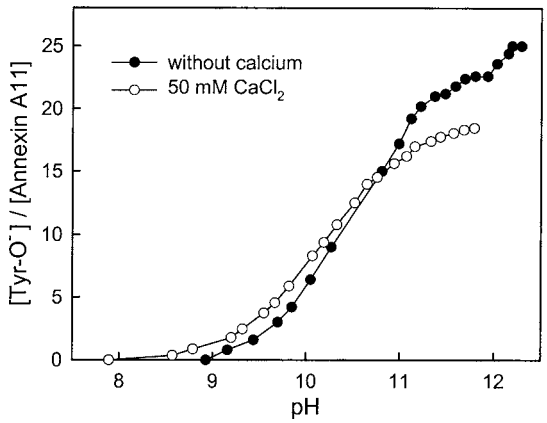

Figure 6 Tyrosine titration of annexin A11

Annexin A11 tyrosine titration was performed by sequential addition of aliquots of 1 M NaOH to a protein sample in 50 mM Tris (pH 8.0) and 0.1 M NaCl and by registration of UV–visible absorption spectra. The number of titrated tyrosine residues was calculated from the variation in absorbance at 295 nm [due to tyrosinate ($Tyr\text{-}O^-$)] relative to protein concentration, either in the absence of calcium (●) or with 50 mM $CaCl_2$ (○).

does not induce artifacts due to the internal filter effect. A gradual decrease in the emission intensity is induced by the quencher without modification in the position of the maximum. Consequently, the tryptophan residue is accessible to acrylamide and must be at least partially exposed. The Stern–Volmer analysis of the variation in the emission intensity at 340 nm as a function of acrylamide concentration is shown in Figure 5(B); the quenching constant calculated from this plot is 12.7 M^{-1}.

Tyrosine titration

Tyrosine titration was achieved by registration of the UV–visible spectra of the recombinant annexin A11, in the absence or presence of 50 mM $CaCl_2$, at increasing pH by the addition of NaOH. At this calcium concentration, binding in the absence of phospholipids should be saturated. Appearance of tyrosinate ($Tyr\text{-}O^-$) residues was followed at 295 nm.

Titration in the absence of calcium distinguishes two main populations of tyrosine residues: buried tyrosine residues with a pK_a of approx. 12 and tyrosine residues, which are at least partially exposed, with a pK_a of approx. 10.5; an additional subpopulation of partially exposed tyrosine residues can also be suggested with a pK_a of 11.6 (Figure 6). Under these conditions, 23 of the 25 tyrosine residues are at least partially exposed. After the addition of 50 mM $CaCl_2$, only 19 of the total 25 tyrosine residues of the protein remain exposed. It was not possible to titrate the buried tyrosine residues because protein aggregates at pH higher than 11.9 in the presence of calcium.

Phospholipid binding and vesicle aggregation

We have analysed the interaction of recombinant annexin A11 with phospholipid vesicles (400 nm) by ultracentrifugation and electrophoretic analysis of the supernatants and pellets either in the absence (1 mM EGTA) or presence of 500 μM $CaCl_2$. Figure 7 shows the result of the analysis using liposomes composed of acidic (PA, PS or PG) and neutral (PC or PE/PC in the ratio 4 : 1) phospholipids. Our results suggest that recombinant annexin A11 is not capable of interacting with PC vesicles in the presence or absence of calcium. However, it is capable of

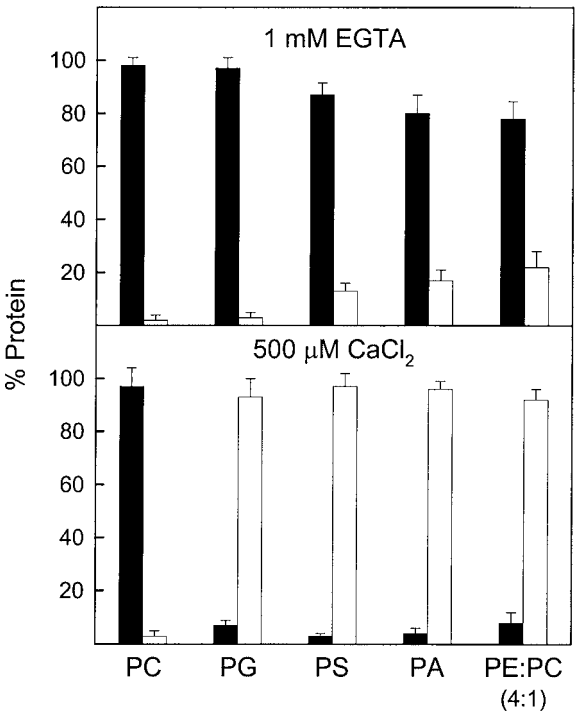

Figure 7 Binding of annexin A11 to phospholipid vesicles

The binding of annexin A11 to 400 nm vesicles with different phospholipid compositions [PC, PG, PS, PA or PE/PC in the ratio 4 : 1] was performed by ultracentrifugation in the absence of calcium (1 mM EGTA) or in the presence of 500 μM $CaCl_2$ and using a lipid/protein molar ratio of 800 : 1. The percentage of annexin A11 in the pellets (white bars) and in the supernatants (black bars) was analysed by SDS/PAGE followed by Western-blot analysis using anti-(annexin A11) antibodies and densitometry of the films.

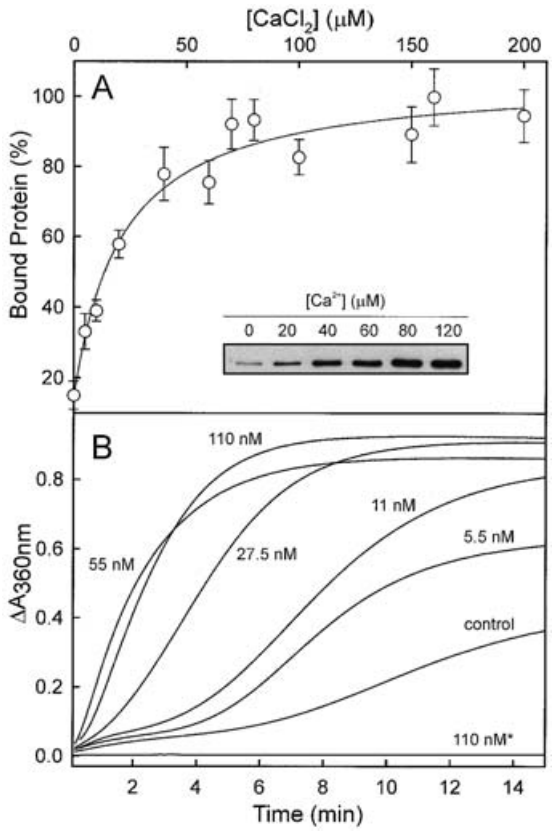

Figure 8 Calcium-dependent aggregation and binding of annexin A11 to PS vesicles

(**A**) Annexin A11 was mixed with PS vesicles (400 nm) at a lipid/protein molar ratio of 800 : 1 in the presence of increasing calcium concentrations. Quantification of the percentage of bound protein was done by ultracentrifugation and SDS/PAGE analysis of the pellets and supernatants, followed either by silver nitrate staining or by immunodetection of annexin A11. The inset shows a representative experiment analysed by Western blot. (**B**) Annexin A11-induced aggregation of PS vesicles (100 nm; 0.1 mg/ml) was followed by monitoring the changes in absorbance at 360 nm at 25 °C after the addition of 1 mM $CaCl_2$. The different protein concentrations are indicated (5.5–110 nM). The self-aggregation of PS vesicles in the presence of 1 mM $CaCl_2$ (control) is also shown. No vesicle aggregation was observed in the presence of 500 μM $CaCl_2$ even at 110 nM protein concentration indicated by an asterisk.

interacting with the neutral phospholipid PE, and with PA, PS and PG, in the presence of 500 μM $CaCl_2$. Furthermore, we have found that annexin A11 interacts in a calcium-independent manner, although to a lower extent, with PE (approx. 22 %) and that there is a certain degree of calcium-independent interaction with PA (approx. 17 %) and PS (approx. 15 %).

A more detailed analysis of the calcium dependence in the interaction of annexin A11 with PS vesicles is shown in Figure 8(A). Approx. 15 % of annexin A11 binds to the vesicles in the absence of calcium, and the bound protein percentage follows a hyperbolic dependence on calcium concentration. At 28 μM $CaCl_2$, 50 % of the total binding to PS vesicles was achieved. Additionally, annexin A11 induces aggregation of PA vesicles at 500 μM $CaCl_2$, but does not induce PS vesicle aggregation at calcium concentrations lower than 1 mM, even at high protein concentrations. Figure 8(B) shows that no aggregation is found at 500 μM $CaCl_2$ using a relatively high annexin A11 concentration (110 nM). At 1 mM $CaCl_2$, slow vesicle aggregation is observed in the absence of annexin, but addition of the protein speeds up this process in a concentration-dependent manner, from 5.5 to 110 nM (Figure 8B).

Spectroscopic analysis of annexin A11 in the presence of phospholipid vesicles

We have analysed the possible conformational changes in annexin A11 after its binding to PS vesicles using CD spectroscopy in the far-UV region (Figure 9A). The addition of PS vesicles (50 nm) in the presence of 1 mM EGTA induces a slight modification of the spectrum, which mainly affects the region between 200 and 210 nm probably due to light-scattering effects. When 200 μM $CaCl_2$ is added to the mixture, a concentration high enough to induce an almost total binding of annexin A11 to PS vesicles, a more significant change is observed in the spectrum with a less negative minimum at 208 nm and an increase in the negative ellipticity at 222 nm. These changes are consistent with an increase in the α-helical content (approx. 9 % according to CCA analysis) and a parallel decrease in the random-coil structure. The CD spectrum of annexin A11 with PC vesicles does not change after the addition of calcium and is almost identical with that obtained with PS in the absence of calcium (results not shown).

The influence of phospholipid vesicles, in the absence or presence of calcium, on the thermal stability of annexin A11 has been analysed by monitoring the changes in molar ellipticity at 220 nm to avoid light-scattering artifacts (Figure 9B). In the absence of vesicles, the T_m of annexin A11 is 45 °C as described above at 208 nm (Figures 3A and 9B). The addition of PS in the absence of calcium does not change this value but involves a loss of co-operativity and a modification in the final state at 80 °C. On the other hand, addition of calcium to a final concentration

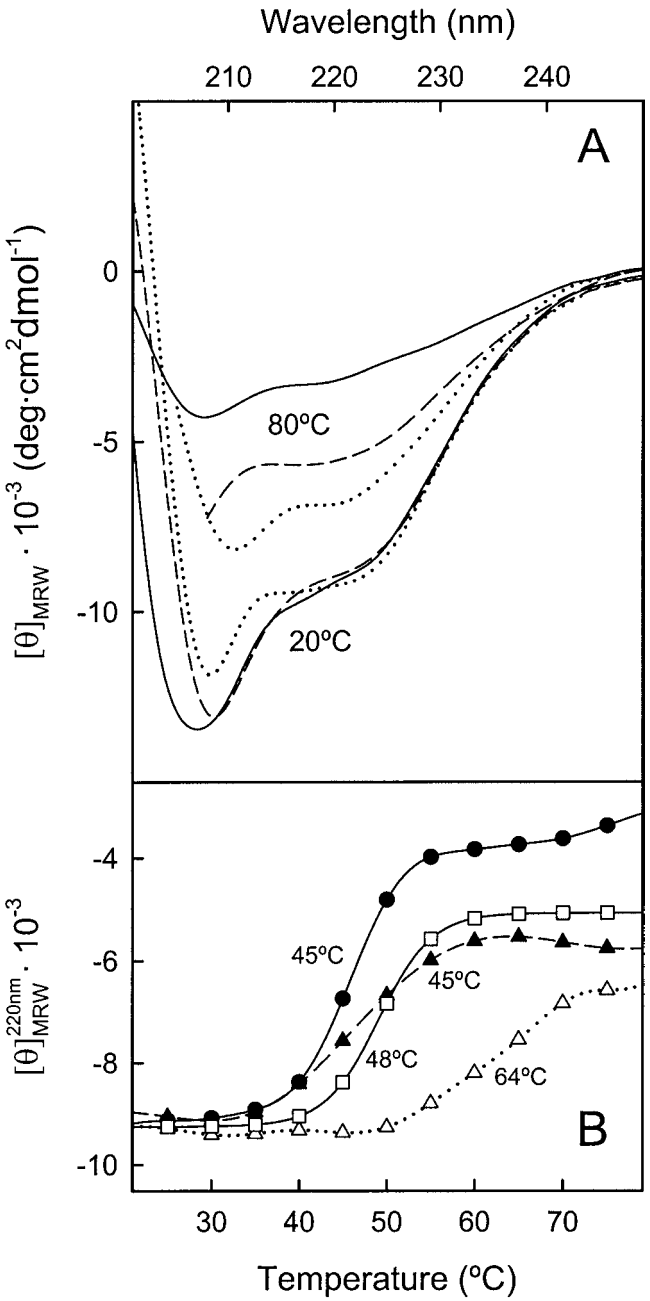

Figure 9 CD analysis of the interaction of PS vesicles with annexin A11

(**A**) Representative far-UV CD spectra of annexin A11 (0.12 mg/ml) in the absence (——) or presence of PS vesicles (molar ratio of lipid/protein is 800 : 1) either without (1 mM EGTA; – – –) or with 200 μM $CaCl_2$ (· · · · · · ·) at 20 and 80 °C. Spectra of annexin A11 with PC vesicles either in the absence or presence of calcium are not shown, as they are almost identical with those with PS vesicles in the presence of 1 mM EGTA. (**B**) Annexin A11 melting curves in the absence (1 mM EGTA; ●) or presence of PS vesicles without (▲) or with 200 μM $CaCl_2$ (△) as well as in the presence of PC vesicles and 200 μM $CaCl_2$ (□). Molar ellipticity/residue was registered at 220 nm; noise reduction was performed using the Standard Analysis software. Melting temperatures determined from the maximum of the first derivative of each curve are also shown.

of 200 μM increases the T_m up to 64 °C; this process is less co-operative and the final denatured state is different. When this analysis is performed under the same experimental conditions but using PC vesicles in the presence of 200 μM $CaCl_2$, only a slight increase in the T_m (approx. 3 °C) is observed.

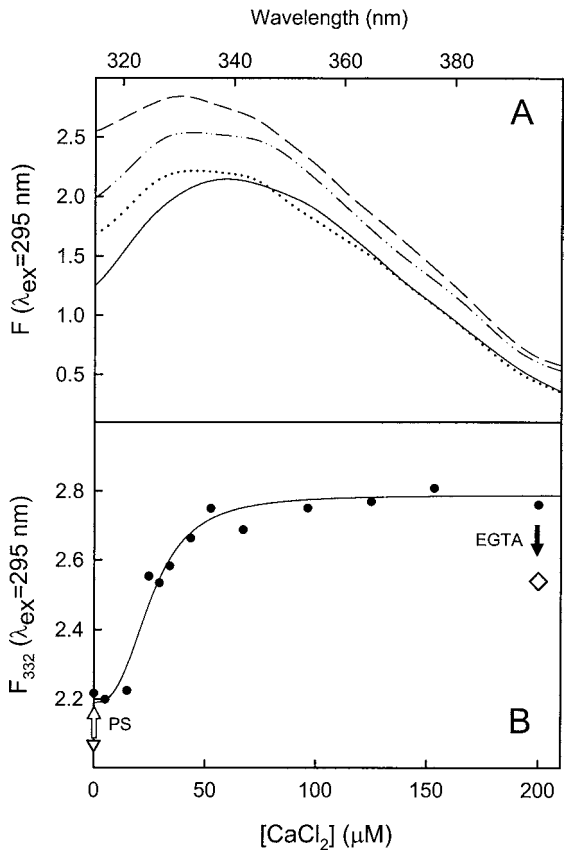

Figure 10 Analysis of the tryptophan fluorescence emission spectra after the binding of annexin A11 to PS vesicles

(**A**) Emission spectra at the excitation wavelength of 295 nm in the absence (——) or presence of PS vesicles without (1 mM EGTA) (· · · · · · ·) and with 200 μM $CaCl_2$ (– – –); – · · – · · – shows the spectra after the addition of EGTA (1 mM final concentration) to the sample with 200 μM $CaCl_2$. All spectra were recorded at 20 °C from 305 to 400 nm. (**B**) Effect of increasing calcium concentration on annexin A11 tryptophan fluorescence intensity at 332 nm in the presence of PS vesicles (●). The fluorescence intensities at 332 nm in the absence of PS vesicles and calcium (▽) and after the addition of PS vesicles (white arrow) and 200 μM $CaCl_2$, followed by addition of EGTA at 1 mM final concentration (black arrow, ◇) are shown.

When annexin A11 is thermally denatured in the absence of phospholipid vesicles, macroscopic aggregation of the protein is observed. However, this process is prevented in the presence of vesicles with or without calcium. Thus the spectra of the denatured protein significantly differ and some secondary structure remains mainly in the presence of calcium and PS, as shown in Figure 9(A).

Fluorescence emission spectra of annexin A11 at an excitation wavelength of 295 nm are shown in Figure 10(A) in the absence or presence of PS vesicles and without (1 mM EGTA) or with 200 μM $CaCl_2$. Addition of vesicles to annexin A11 induces a shift in the position of the emission maximum from approx. 340 to 332 nm. Addition of calcium does not modify this wavelength but increases the tryptophan quantum yield. The variation in fluorescence intensity at 332 nm with calcium concentration shows a midpoint effect at 25 μM $CaCl_2$ (Figure 10B). In Figure 10(B), the inverted triangle indicates the emission intensity in the absence of phospholipids (lower due to the maximum position shift), and the diamond indicates the decrease in intensity achieved by the addition of EGTA (1 mM final concentration) to the sample with PS vesicles and 200 μM $CaCl_2$. The changes

in the fluorescence emission spectrum are not fully reversible after removal of calcium, as the tryptophan maximum remains at 332 nm and only a slight decrease in the quantum yield is observed.

Structural model

The sequence and deduced secondary structure of annexin A11 were expanded into a multiple-sequence alignment to facilitate comparative and evolutionary studies, and a virtual three-dimensional model was created by sequence-threading through the crystallography coordinates of known annexin structures. Annexin A11 homologues, identified in 20 vertebrate species, are represented by the mammal, bird, amphibian and fish proteins aligned in Figure 11(A). The greater sequence variability, alignment gaps and unique amino acid composition of the N-termini are evident, with an increased percentage of proline (28 %), glycine (20 %) and tyrosine (9 %) and a tryptophan residue (Trp^{23}), which contrast with conserved type II calcium-binding sites and congruent structures of the tetrad core, in spite of the evolutionary distances between these species. Secondary-structure predictions (http://www.expasy.org) determined that the N-terminus would be expected to adopt a random-coil conformation except for one short α-helical segment ('h' strings in Figure 11A), whereas each tetrad core repeat contains the five α-helices common to other annexins. The observation that the 12 paralogous human annexins exhibit only 45–55 % amino acid identity suggested that subfamily differences might be accounted for by variable sites non-critical for function as well as by synaptomorphic sites under functional constraint acting as determinants of subfamily specificity. Although annexin A11 was an ancestral progenitor of other paralogous annexins and thus shares many features in common [16], we sought to identify sites uniquely conserved among annexin A11 members. The DIVERGE v1.04 program from Gu [38] (available at http://www.phyba.iastate.edu/) computed 'evolutionary impact' values for each residue in a global sequence alignment and identified Cys^{224} and Cys^{409} as structurally relevant differences from other annexins with high divergence impact that implied functional specificity for annexin A11. Together with four other cysteine residues common to other annexins, these may contribute additional structural stability and redox susceptibility to annexin A11 members.

A three-dimensional model of annexin A11 was generated using the DeepView/Swiss-PdbViewer v3.7 computer program [39] and the Swiss-Model server (http://www.expasy.org/). These utilized public X-ray crystallography data [40] for full-length pig annexin A1 and human and rat annexin A5 (Protein Data Bank entries 1MCX, 1ANX and 1A8A) in the 'high-calcium' form to thread the mouse annexin A11 amino acid sequence into a three-dimensional model for the homologous tetrad core region (Figure 11B). This representation serves to illustrate the spatial proximity between residues and domains that might otherwise appear distant in sequence alignment format. Thus the residues involved in the type II calcium binding to phospholipids (mkGxGT-38aa-D/E) appear co-ordinated on the external convex surface of the molecule near Cys^{409}, whereas the N-terminus (where Trp^{23} is located) is orientated towards the opposite, concave (cytosolic) side of the molecule. DeepView program identified four tyrosine residues classified as not exposed to the solvent and within potentially buried α-helical coils: Tyr^{312} and Tyr^{471} (< 1 % exposure); Tyr^{491} (< 2 %); and Tyr^{396} (< 4 %) (Figure 11A). Thus it is highly probable that these residues are among those showing a higher pK_a value in the tyrosine titration in the presence of calcium. The other five core tyrosine residues were predicted to be exposed (24–28 % exposure). When the three-dimensional model of annexin A11 was obtained by comparison with the only known annexin X-ray structure in the absence of calcium (full-length pig annexin A1; PDB entry 1HM6), only Tyr^{312} and Tyr^{471} were predicted to be completely buried (< 1 % exposure); Tyr^{491} and Tyr^{396} present approx. 10 and 15 % exposure respectively. The interchangeability of Tyr and Phe at certain positions between fish and higher vertebrates suggests the functional importance of bulky and/or hydrophobic residues at these positions relative to the interloop calcium-binding ligands. This model is consistent with our experimental findings and testifies to the structural relevance of uncharged cysteine and tyrosine residues to annexin function.

DISCUSSION

The eukaryotic annexin superfamily has been widely studied since the identification of its first members 25 years ago. The resolution of the crystal structure of some of these proteins with a short or truncated N-terminal extension [7,41–43] has provided a detailed structural knowledge of the core domain and the effects of calcium binding on this structure. However, the structural diversity of N-termini and the disparate functions assigned to these proteins emphasize the significant contribution of this distinctive extension to the functional divergence of animal annexins. The N-terminus is therefore considered to be a specific regulatory domain of annexins [1–3], although its structure and relationship with the core domain still remain poorly understood. Whereas the 314-amino-acid tetrad core region of annexin A11 is highly conserved, its extensive N-terminal region varies in length among vertebrate members (171–221 residues) and presents a high content of proline, glycine and tyrosine residues [21,22]. These unusual features aroused our interest in performing a structural study of annexin A11.

Annexin A11 has been isolated previously from bovine and rabbit lung [22,44] or as a fusion protein with glutathione S-transferase or with the mannose-binding protein [27,31]. However, to perform a spectroscopic characterization, the protein should be similar to the wild-type form and relatively large amounts of purified protein were required. We achieved a high yield in the expression of soluble annexin A11 in *E. coli* by the addition of a His tag, even though approx. 50 % of the protein remains insoluble in the cell homogenate. This insertion also minimizes the extent of degradation and simplifies the purification process via affinity chromatography, which further removes N-terminally degraded forms. The requirement for chelating agents to prevent precipitation when imidazole is removed after the chromatography points out that the His tag is capable of inducing autoaggregation of annexin A11, acting as a bridge between different molecules in the presence of cations such as Ni^{2+} or Ca^{2+}. Although the addition of calcium induces aggregation of the protein containing the His tag, this does not occur when the tag is removed. The use of reducing agents throughout the purification procedure prevents the oxidation of the redox-sensitive free cysteine residues that seem to be important for annexin A11 function, as mentioned above. Recombinant annexin A11 was obtained with only small modifications from the wild-type, a change in position 2 from Ser to Gly and the addition of Gly-Ala at the N-terminus, which are not likely to have any effect on the structure or functional properties of annexin A11.

The main secondary-structure element present in the highly conserved annexin core is the α-helix [7–10]. Accordingly, the CCA analysis of the CD spectrum of annexin A5, which possesses a very short N-terminus of 15 amino acid residues and whose

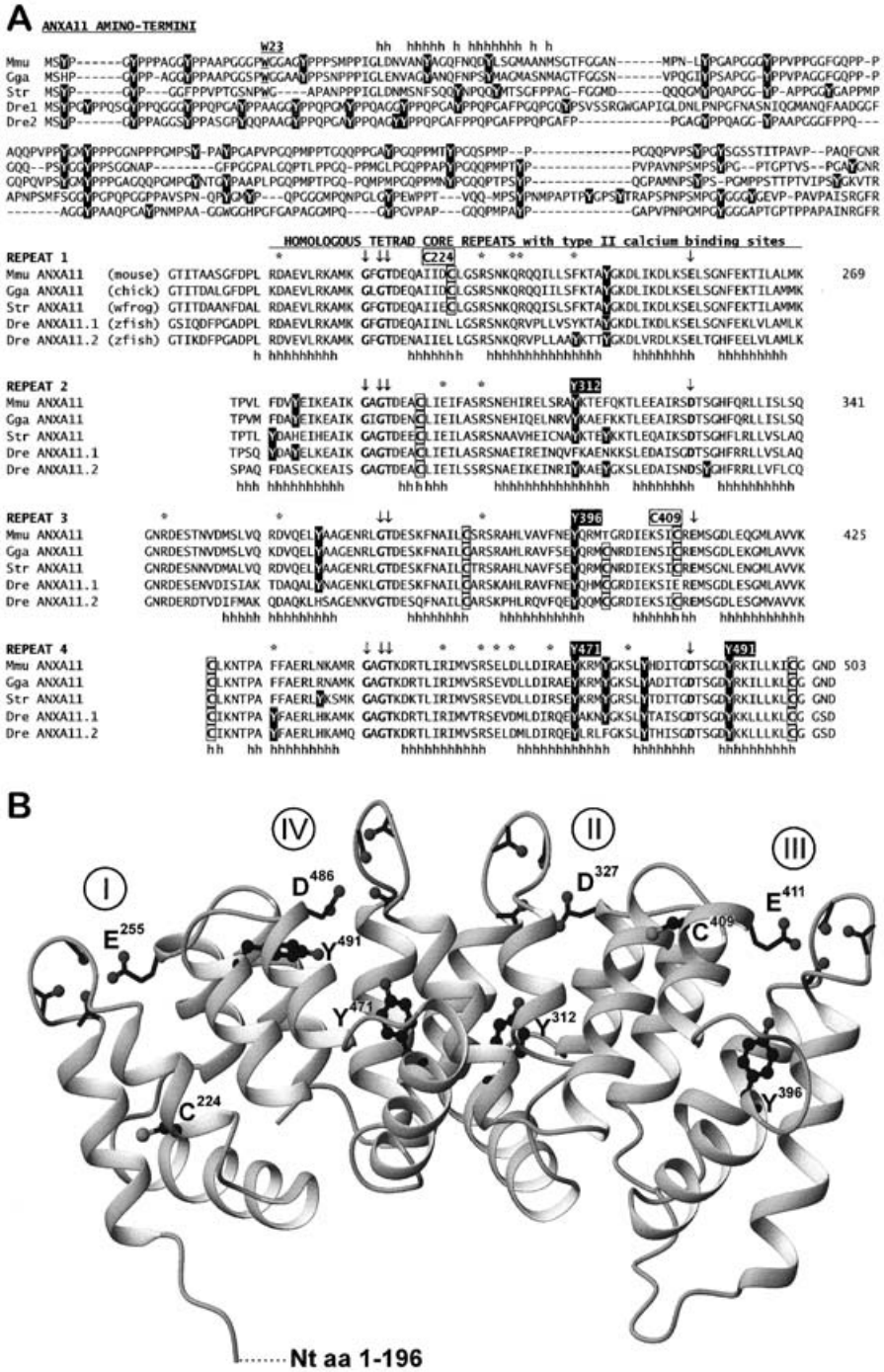

Figure 11 Annexin A11 sequence alignment and three-dimensional model

(**A**) Amino acid sequence alignment of annexin A11 from species representing mammal (Mmu, mouse, *Mus musculus*), bird (Gga, chicken, *Gallus gallus*), amphibian (Str, western clawed frog, *Silurana tropicalis*) and fish duplicate genes (Dre, zebrafish, *Danio rerio*). The N-termini (top panels) contain Trp^{23} and increased proline, glycine and tyrosine content, whereas the four homologous repeats of the tetrad core region below identify conserved cysteine residues (boxed), tyrosine residues (reverse-shaded), type II calcium-binding motifs 'mkGxGT-38aa-D/E' (beneath arrows) and residues highly preserved in all annexins (indicated by asterisks). The 'h' clusters in each repeat correspond to the five α-helical loops A, B, C, D and E. (**B**) A three-dimensional protein model of the homologous tetrad core of mouse annexin A11 was derived by sequence threading through X-ray crystallography coordinates of pig annexin A1 and human and rat annexin A5 by DeepView/SwissPDB v3.7 [39] and SwissModel (available at http://www.expasy.org/). The predominant α-helical backbone structure portrays the four major calcium co-ordination sites on the upper convex surface, together with strategically located cysteine and tyrosine residues. The carbonyl groups and acid residues proposed to be involved in calcium co-ordination are shown. The attachment origin 187 for the non-homologous N-terminus (not shown in full) extends from the lower concave side. The Figure was prepared using the MOLMOL program [54].

crystal structure is well known, shows over 70% of α-helix [9,10,35]. This is not the case for annexin A11, as can be easily observed from the comparison of the spectrum with that of annexin A5. CCA analysis reveals three main contributions: α-helix (29%), random coil (31%) and β-turns (26%). The remaining 14% is assigned to extended β-strands; however, this percentage must arise from artifacts derived from the application of the CCA, since secondary-structure predictions based on the

amino acid sequence indicate a very low theoretical percentage of these structures. There are no structural studies concerning this annexin, but the structural features of the core domain and the relatively high degree of similarity to other annexins of known three-dimensional structure suggest that the α-helical contribution probably arises from the protein core. From the studies performed with the N-terminus, the existence of an α-helix involved in S100A6 binding has been suggested [27,45], in a way similar to those described for p53 with S100B, and annexins A1 and A2 with S100A11 and S100A10 respectively [28–30].

According to the secondary-structure predictions based on the amino acid sequence of the N-terminal extension, this region would be mainly in random coil except for the theoretical amphipathic α-helix. However, the particular amino acid sequence of the N-terminus (rich in glycine, proline, tyrosine and glutamine) suggests the formation of poly(Pro) β-turn helices that would be responsible for the high β-turn percentage detected. These atypical secondary structures have been detected in the N-terminus of annexin A7 [46], whose sequence, although shorter, is quite similar to that of annexin A11. Accordingly, the N-terminus would account for both random-coil and β-turn contributions predicted from the CD spectra.

In general, the annexin core domain is known to be quite stable, with a higher T_m for those annexins with a short N-terminus [10]. The presence of a long N-terminal extension could induce a destabilization of the core domain. In fact, the T_m for annexin A11 is approx. 6 °C lower than that of human annexin A5, which has one of the lowest T_m among mammalian annexins. The change in the negative molar ellipticity at 208 nm with increase in temperature is mainly a reflection of α-helices unfolding to unordered structure. As the melting curve shows only one co-operative transition, the unfolding of the protein core and any hypothetical α-helix from the N-terminus must take place simultaneously.

Calcium binding does not greatly affect the CD spectrum of annexin A11. For other members of the family, the secondary-structure changes described after calcium binding are also small, implying mainly three-dimensional modifications of the calcium–phospholipid-binding sites with an increase in the percentage of α-helix and a rearrangement of the protein core [9,10,47]. The analysis of the CD spectra of annexin A11 reveals a hyperbolic increase in the ratio between molar ellipticities at 222 and 206.5 nm with calcium concentration. On calcium binding, this ratio increases towards that of pure α-helix, pointing to a higher contribution of this structure with a concomitant decrease in random coil. This hypothesis is also supported by the CCA analyses of the spectra, which suggest a 5–6% increase in α-helix with an equivalent decrease in random coil. Even though it has been described that saturation with calcium of annexins with short N-termini induces a similar increase in the percentage of α-helix [9,10], the total number of residues involved should be considered. Thus, whereas only 16–19 residues change in annexin A5 core, 25–30 residues may become α-helical in annexin A11. Owing to the structural similarity among the protein cores in different annexins, the increase in the α-helical content in annexin A11 cannot be completely explained by the conformational rearrangements of the protein core, and probably involves changes in its N-terminus as well.

In contrast with the relatively small conformational changes observed, calcium induces a great thermal stabilization, increasing the T_m by approx. 14 °C. This increase is larger than that observed for other mammalian annexins such as human annexin A5 (approx. 10 °C) [10]. Moreover, the calcium-bound states of annexin A5 and annexin A11 have a similar thermal stability, whereas calcium-free annexin A11 shows a lower stability. Taking into account the degree of homology of the annexin core, differences, quite probably in the N-terminal region, are responsible for the changes in protein stability. Therefore we propose that the long N-terminus in annexin A11 has a destabilizing effect in the calcium-free state; structural changes after calcium binding contribute to stabilization of the protein and the T_m of annexin A11 approaches that of annexin A5. It remains to be explained how this interaction could take place, but it is tempting to speculate with a mechanism resembling that described for annexin A1 [8]. This annexin binds to S100A11 through an amphipathic α-helix, which, in a calcium-free state, inserts into domain III, displacing helix 3D. The full-length crystal structure of annexin A1 has been obtained recently, showing that calcium binding induces the refolding of helix 3D pushing the N-terminus outside the annexin core [48], thus enabling the interaction with S100A11. In addition to the stabilizing effects, this mechanism also involves an increase in α-helix due to the refolding of helix 3D.

Tertiary structure analysis through fluorescence studies reveals that Trp^{23} is completely exposed to the polar solvent either in the presence or absence of calcium, as the maximum of emission remains at 340 nm under both conditions and there is no decrease in intensity due to calcium binding. Acrylamide quenching also supports this observation, as the obtained Stern–Volmer constant is 12.7 M^{-1}, characteristic of an almost totally exposed tryptophan residue. Whereas free tryptophan residues or *N*-acetyl-tryptophan-amide show a K_{SV} of approx. 16 $\cdot M^{-1}$, exposed tryptophan residues in proteins present values between 10 and 14 M^{-1} [49]. On the other hand, tyrosine emission decreases with increase in calcium concentration. This decrease is probably due to a change in the microenvironment of some tyrosine residues to a more hydrophobic one, where interactions that stabilize the polar group of this residue result in the quenching of emission. To confirm this observation, tyrosine titration was performed in the calcium-free and calcium-bound state. According to the titration, in the absence of calcium two tyrosine residues are buried, whereas the calcium-bound state presents six buried tyrosine residues. Therefore the addition of calcium induces a conformational change in annexin A11 that implies the translocation of some tyrosine residues from a polar to a hydrophobic environment, whereas Trp^{23} remains unaltered. Taking into account the similarity between the putative amphipatic α-helix in the N-terminus of annexin A11 and that described in the N-terminus of annexin A1, one could speculate that the N-terminus would be even more exposed to the solvent in the presence of calcium. Thus at least some of the tyrosine residues internalized in the presence of calcium are probably located in the protein core. This hypothesis is strongly supported by the surface analysis of the proposed structural model, where the highly conserved residues 312, 396, 471 and 491 are predicted to be buried in the protein core. Among these residues, Tyr^{312} and Tyr^{396} could be the ones buried in the calcium-free state, as they are the only ones predicted as buried in the calcium-free model. It is not possible to locate the remaining two tyrosine residues titrated as internal in the presence of calcium, as the three-dimensional models cannot predict the structure and position of the N-terminus.

Functionally, annexin A11 interacts with acidic phospholipid and PE vesicles in a calcium-dependent fashion, whereas no binding is observed with PC, as shown previously with wild-type annexin A11 [22]. Partial binding in the absence of calcium was observed to PE, PA and PS vesicles as described for other annexins [50–52]. Phospholipid specificity is generally conserved in calcium-independent binding, and

this is likely to be the case for annexin A11. There must be two contributions to the interaction with phospholipids under these conditions: a specific polar recognition and a hydrophobic interaction. The N-terminus of annexin A11 may be able to insert into the bilayer and establish hydrophobic contacts with the phospholipids, but this would imply a reorientation of the N-terminus from the concave/cytosolic side towards the cell membrane.

Binding of annexin A11 to PS vesicles shows a hyperbolic dependence on calcium concentration. The interaction requires calcium concentrations in the micromolar range, with 50% binding achieved at 28 μM. Consequently, there is a great increase in calcium affinity in the presence of phospholipids as has been observed for other annexins [1,2,47]. Calcium requirement for PS binding of annexin A11 is higher than that of annexin A2 and lower than that for annexin A5 [1]. These differences could account for the development of divergent functions throughout vertebrate evolution. Annexin A11 induces PS vesicle aggregation only at non-physiological calcium concentrations (>1 mM) at which this cation itself acts as a bridge for vesicle aggregation. However, annexin A11 is able to accelerate the aggregation process in a protein concentration-dependent manner. These results formulate a role for annexin A11 in aggregation processes *in vivo*, where the presence of other proteins such as S100A6 could modify calcium requirements, as described for other annexins. For example, calcium requirement of annexin A2 for the induction of vesicle aggregation is significantly reduced in the presence of S100A10 [53].

Spectroscopic analyses of the interaction of annexin A11 with PS vesicles give further support to the above observations. Addition of PS vesicles in the absence of calcium induces only a small change in the CD spectrum, which does not affect the thermal stability of the protein, although a loss of co-operativity in the melting curve is observed. Taking into account that annexin A11 is capable of interacting weakly with PS in a calcium-independent manner, this interaction could be responsible for the observed conformational change. However, CD spectroscopy shows that annexin A11 suffers a conformational rearrangement after vesicle binding in the presence of calcium. Calcium-dependent binding to PS vesicles induces an increase in α-helical content similar to the addition of calcium in the absence of phospholipids, but to a higher extent (approx. 9% versus 5–6%). The observed change is again too large to be exclusively due to changes in the protein core; therefore the N-terminus is likely to be involved in this process.

Calcium-dependent binding to PS vesicles is also accompanied by a large increase (approx. 20 °C) in thermal stability, higher than that described for calcium binding alone, and the loss of co-operativity is also remarkable. All these changes must be the consequence of a strong specific interaction, as they are not observed when using PC vesicles. In this case, the small increase in T_m could be due only to binding of calcium to the protein without interaction with the vesicles, and thus no loss of co-operativity is displayed.

In addition to these results, fluorescence studies support a role of the N-terminus in both calcium-independent and calcium-dependent interactions with PS vesicles. The environment of the N-terminal Trp^{23} was modified when vesicles were added to the protein preparation in the absence of calcium, with a significant blue-shift in the emission maximum corresponding to a change from an almost total exposure to the solvent to a more hydrophobic environment. However, taking into account that the quantum yield was not modified significantly, this residue probably remained partially in contact with the solvent. Once again, this observation supports the notion of a weak calcium-independent interaction, probably through the N-terminus of annexin A11 establishing hydrophobic contacts with the bilayer.

Addition of calcium to the annexin/vesicle mixture is characterized by an increase in the tryptophan quantum yield, which presents a midpoint effect almost coincident to that observed in the ultracentrifugation studies. This increase is probably due to the insertion of Trp^{23} into the lipid bilayer, which would protect this residue from solvent quenching. Furthermore, the addition of excess EGTA is not able to reverse the interaction, so there must be a hydrophobic component in the binding that accounts for this effect.

This original structural characterization of annexin A11 reveals that the N-terminus, the longest of all known mammalian annexins and containing unusual composition and repeat patterns, contributes significantly to the overall annexin structure. The analysis of the structural conservation of annexin A11 using a combination of primary- and secondary-structure analyses, three-dimensional models and the evolutionary divergence offers a novel insight into its key functional determinants. This annexin has one of the lowest melting temperatures *in vitro* (45 °C) and calcium binding promotes subtle rearrangements in the secondary and tertiary structures of the protein to induce significant thermal stabilization. The recombinant protein binds to acidic phospholipids in a calcium-dependent manner as described for other annexins; it also shows calcium-independent binding, but to a lower extent. These results suggest that the binding of annexin A11 to PS vesicles presents both hydrophobic and polar contributions due to the N-terminus and the annexin core respectively. According to the spectroscopic data, a two-step mechanism can be proposed. First, a weak interaction is established through surface hydrophobic contacts with some degree of polar specificity; secondly, after the addition of calcium, a tight binding to the lipid bilayer takes place, enabling in this way the partial insertion of the N-terminus, which reinforces the interaction. It remains however to be determined whether calcyclin, sorcin or ALG-2 interaction with annexin A11 will influence its binding to lipid bilayers.

We are grateful to Dr Hiroyoshi Hidaka for kindly providing a polyclonal antibody raised against bovine annexin A11. This work was supported by grant nos. PM98-0083, PB98-1529 and BMC2002-01407 from the Dirección General de Investigación (Spain).

REFERENCES

1 Raynal, P. and Pollard, H. B. (1994) Annexins: the problem of assessing the biological role for a gene family of multifunctional calcium- and phospholipid-binding proteins. Biochim. Biophys. Acta **1197**, 63–93
2 Swairjo, M. A. and Seaton, B. A. (1994) Annexin structure and membrane interactions: a molecular perspective. Annu. Rev. Biophys. Struct. **23**, 193–213
3 Gerke, V. and Moss, S. E. (2002) Annexins: from structure to function. Physiol. Rev. **82**, 331–371
4 Morgan, R. O. and Fernandez, M. P. (1998) Expression profile and structural divergence of novel human annexin 31. FEBS Lett. **434**, 300–304
5 Liemann, S. and Huber, R. (1997) Three-dimensional structure of annexins. Cell. Mol. Life Sci. **53**, 516–521
6 Morgan, R. O., Jenkins, N. A., Gilbert, D. J., Copeland, N. G., Balsara, B. R., Testa, J. R. and Fernandez, M. P. (1999) Novel human and mouse annexin A10 are linked to the genome duplications during early chordate evolution. Genomics **60**, 40–49
7 Huber, R., Römisch, J. and Pâques, E. P. (1990) The crystal and molecular structure of human annexin V, an anticoagulant protein that binds to calcium and membranes. EMBO J. **9**, 3867–3873
8 Rosengarth, A., Gerke, V. and Luecke, H. (2001) X-ray structure of full-length annexin 1 and implications for membrane aggregation. J. Mol. Biol. **306**, 489–498
9 Arboledas, D., Olmo, N., Lizarbe, M. A. and Turnay, J. (1997) Role of the N-terminus in the structure and stability of chicken annexin V. FEBS Lett. **416**, 217–220
10 Turnay, J., Olmo, N., Gasset, M., Iloro, I., Arrondo, J. L. R. and Lizarbe, M. A. (2002) Calcium-dependent conformational rearrangements and protein stability in chicken annexin A5. Biophys. J. **83**, 2280–2291

11 Burger, A., Berendes, R., Liemann, S., Benz, J., Hofman, A., Göttig, P., Huber, R., Gerke, V., Carsten, T., Römisch, J. et al. (1996) The crystal structure and ion channel activity of human annexin II, a peripheral membrane protein. J. Mol. Biol. **257**, 839–847
12 Rosengarth, A., Rösgen, J., Hinz, H. J. and Gerke, V. (1999) A comparison of the energetics of annexin I and annexin V. J. Mol. Biol. **288**, 1013–1025
13 Morgan, R. O. and Fernandez, M. P. (1995) Molecular phylogeny of annexins and identification of a primitive homologue in *Giardia lamblia.* Mol. Biol. Evol. **12**, 967–979
14 Fernandez, M. P., Jenkins, N. A., Gilbert, D. J., Copeland, N. G. and Morgan, R. O. (1996) Sequence and chromosomal localization of mouse annexin XI. Genomics **37**, 366–374
15 Morgan, R. O., Bell, D. W., Testa, J. R. and Fernandez, M. P. (1998) Genomic locations of ANX11 and ANX13 and the evolutionary genetics of human annexins. Genomics **48**, 100–110
16 Bances, P., Fernández, M. R., Rodríguez-García, M. I., Morgan, R. O. and Fernandez, M. P. (2000) Annexin A11 (ANXA11) gene structure as the progenitor of paralogous annexins and source of orthologous cDNA isoforms. Genomics **69**, 95–103
17 Iglesias, J. M., Morgan, R. O., Jenkins, N. A., Copeland, N. G., Gilbert, D. J. and Fernandez, M. P. (2002) Comparative genetics and evolution of annexin A13 as the founder gene of vertebrate annexins. Mol. Biol. Evol. **19**, 608–618
18 Towle, C., Weissbach, L. and Treadwell, B. V. (1992) Alternatively spliced annexin XI transcripts encode proteins that differ near the amino-terminus. Biochim. Biophys. Acta **1131**, 223–226
19 Fiedler, K., Lafont, F., Parton, R. G. and Simons, K. (1995) Annexin XIIIb: a novel epithelial specific annexin is implicated in vesicular traffic to the apical plasma membrane. J. Cell Biol. **128**, 1043–1053
20 Sable, C. L. and Riches, D. W. H. (1999) Cloning and functional activity of a novel truncated form of annexin IV in mouse macrophages. Biochem. Biophys. Res. Commun. **258**, 162–167
21 Towle, C. A. and Treadwell, B. V. (1992) Identification of a novel mammalian annexin. cDNA cloning, sequence analysis, and ubiquitous expression of the annexin XI gene. J. Biol. Chem. **267**, 5416–5423
22 Tokumitsu, H., Mizutani, A., Minami, H., Kobayashi, R. and Hidaka, H. (1992) A calcyclin-associated protein is a newly identified member of the Ca^{2+}/phospholipid-binding proteins, annexin family. J. Biol. Chem. **267**, 8919–8924
23 Iino, S., Sudo, T., Niwa, T., Fukasawa, T., Hidaka, H. and Niki, I. (2000) Annexin XI may be involved in Ca^{2+}- or GTP-γS-induced insulin secretion in the pancreatic β-cell. FEBS Lett. **479**, 46–50
24 Misaki, Y., Pruijn, G. J. M., van der Kemp, A. W. C. M. and van Venrooij, W. J. (1994) The 56K autoantigen is identical to human annexin XI. J. Biol. Chem. **269**, 4240–4246
25 Mizutani, A., Watanabe, N., Kitao, T., Tokumitsu, H. and Hidaka, H. (1995) The long amino-terminal tail domain of annexin XI is necessary for its nuclear localization. Arch. Biochem. Biophys. **318**, 157–165
26 Furge, L. L., Chen, K. and Cohen, S. (1999) Annexin VII and annexin XI are tyrosine phosphorylated in peroxovanadate-treated dogs and in platelet-derived growth factor-treated rat vascular smooth muscle cells. J. Biol. Chem. **274**, 33504–33509
27 Sudo, T. and Hidaka, H. (1999) Characterization of the calcyclin (S100A6) binding site of annexin XI-A by site-directed mutagenesis. FEBS Lett. **444**, 11–14
28 Mäler, L., Sastry, M. and Chazin, W. J. (2002) A structural basis for S100 protein specificity derived from comparative analysis of apo and Ca^{2+}-calcyclin. J. Mol. Biol. **317**, 279–290
29 Réty, S., Sopkova, J., Renouard, M., Osterloh, D., Gerke, V., Tabaries, S., Russo-Marie, F. and Lewit-Bentley, A. (1999) The crystal structure of a complex of p11 with the annexin II N-terminal peptide. Nat. Struct. Biol. **6**, 89–95
30 Réty, S., Osterloh, D., Arié, J. P., Tabaries, S., Seemann, J., Russo-Marie, F., Gerke, V. and Lewit-Bentley, A. (2000) Structural basis of the Ca^{2+}-dependent association between S100C (S100A11) and its target, the N-terminal part of annexin I. Structure Fold. Res. **8**, 175–184
31 Satoh, H., Shibata, H., Nakano, Y., Kitaura, Y. and Maki, M. (2002) ALG-2 interacts with the amino-terminal domain of annexin XI in a Ca^{2+}-dependent manner. Biochem. Biophys. Res. Commun. **291**, 1166–1172
32 Brownawell, A. M. and Creutz, C. E. (1997) Calcium-dependent binding of sorcin to the N-terminal domain of synexin (annexin VII). J. Biol. Chem. **272**, 22182–22190
33 Gómez-Guillén, M. C., Turnay, J., Fernández-Díaz, M. D., Olmo, N., Lizarbe, M. A. and Montero, P. (2002) Structural and physical properties of gelatine extracted from different marine species: a comparative study. Food Hydrocolloids **16**, 25–34
34 Perczel, A., Park, K. and Fasman, G. D. (1992) Analysis of the circular dichroism spectrum of proteins using the convex constraint algorithm: a practical guide. Anal. Biochem. **203**, 83–93
35 Turnay, J., Pfannmüller, E., Lizarbe, M. A., Bertling, W. and von der Mark, K. (1995) Collagen binding activity of recombinant and N-terminally modified annexin V (anchorin CII). J. Cell. Biochem. **58**, 208–220
36 Laemmli,U. K. (1970) Cleavage of structural proteins during the assembly of the head of bacteriophage T4. Nature (London) **227**, 680–685
37 Turnay, J., Olmo, N., Lizarbe, M. A. and von der Mark, K. (2002) Changes in the expression of annexin A5 gene during *in vitro* chondrocyte differentiation: influence of cell attachment. J. Cell. Biochem. **84**, 132–142
38 Gu, X. (1999) Statistical methods for testing functional divergence after gene duplication. Mol. Biol. Evol. **16**, 1664–1674
39 Guex, N., Diemand, A. and Peitsch, M. C. (1999) Protein modelling for all. Trends Biol. Sci. **24**, 364–367
40 Berman, H. M., Westbrook, J., Feng, Z., Gilliland, G., Bhat, T. N., Weissig, H., Shindyalov, I. N. and Bourne, P. E. (2000) The protein data bank. Nucleic Acids Res. **28**, 235–242
41 Weng, X., Luecke, H., Song, I. S., Kang, D. S., Kim, S. H. and Huber, R. (1993) Crystal structure of human annexin I at 2.5 Å resolution. Protein Sci. **2**, 448–458
42 Bewley, M. C., Boustead, C. M., Walker, J. H. and Huber, R. (1993) Structure of chicken annexin V at 2.25-Å resolution. Biochemistry **32**, 3923–3928
43 Luecke, H., Chang, B. T., Mailliard, W. S., Schlaepfer, D. D. and Haigler, H. T. (1995) Crystal structure of the annexin XII hexamer and implications for bilayer insertion. Nature (London) **378**, 512–515
44 Mizutani, A., Usuda, N., Tokumitsu, H., Minami, H., Yasui, K., Kobayashi, R. and Hidaka, H. (1992) CAP-50, a newly identified annexin, localizes in nuclei of cultured fibroblast 3Y1 cells. J. Biol. Chem. **267**, 13498–13504
45 Tokumitsu, H., Mizutani, A. and Hidaka, H. (1993) Calcyclin-binding site located on the NH_2-terminal domain of rabbit CAP-50 (annexin XI): functional expression of CAP-50 in *Escherichia coli.* Arch. Biochem. Biophys. **303**, 302–306
46 Matsushima, N., Creutz, C. E. and Kretzinger, R. H. (1990) Polyproline, β-turn helices. Novel secondary structures proposed for the tandem repeats within rhodopsin, synaptophysin, synexin, gliadin, RNA polymerase II, hordein, and gluten. Proteins **7**, 125–155
47 Sopkova, J., Vincent, M., Takahashi, M., Lewit-Bentley, A. and Gallay, J. (1999) Conformational flexibility of domain III of annexin V at membrane/water interfaces. Biochemistry **38**, 5447–5458
48 Rosengarth, A. and Luecke, H. (2003) A calcium-driven conformational switch of the N-terminal and core domains of annexin A1. J. Mol. Biol. **326**, 1317–1325
49 Lakowicz, J. R. (1999) Quenching of fluorescence. In Principles of Fluorescence Spectroscopy, 2nd edn (Lakowicz, J. R., ed.), pp. 237–265, Kluwer Academic/Plenum, New York
50 Jost, M., Zeuschner, D., Seemann, J., Weber, K. and Gerke, V. (1997) Identification and characterization of a novel type of annexin–membrane interaction: Ca^{2+} is not required for the association of annexin II with endosomal membranes. Biochim. Biophys. Acta **110**, 221–228
51 König, J. and Gerke, V. (2000) Modes of annexin–membrane interactions analyzed by employing chimeric annexin proteins. Biochim. Biophys. Acta **1498**, 174–180
52 Tzima, E. and Walker, J. H. (2000) Platelet annexin V: the ins and outs. Platelets **11**, 245–251
53 Lambert, O., Gerke, V., Bader, M. F., Porte, F. and Brisson, A. (1997) Structural analysis of junctions formed between lipid membranes and several annexins by cryo-electron microscopy. J. Mol. Biol. **272**, 42–55
54 Koradi, R., Billeter, M. and Wüthrich, K. (1996) MOLMOL: a program for display and analysis of macromolecular structures. J. Mol. Graph. **14**, 51–55

Received 4 November 2002/10 March 2003; accepted 11 April 2003
Published as BJ Immediate Publication 11 April 2003, DOI 10.1042/BJ20021721